PHYSICAL REVIEW B **89**, 140102(R) (2014)

Shock waves in polycrystalline iron: Plasticity and phase transitions

Nina Gunkelmann,[1,2] Eduardo M. Bringa,[3,4] Diego R. Tramontina,[3] Carlos J. Ruestes,[3] Matthew J. Suggit,[5] Andrew Higginbotham,[5] Justin S. Wark,[5] and Herbert M. Urbassek[1,*]

[1]*Physics Department and Research Center OPTIMAS, University Kaiserslautern, Erwin-Schrödinger-Straße, D-67663 Kaiserslautern, Germany*

[2]*Institute for Multiscale Simulations, Friedrich-Alexander-Universität, D-91052 Erlangen, Germany*

[3]*Instituto de Ciencias Básicas, Universidad Nacional de Cuyo, Mendoza, 5500 Argentina*

[4]*CONICET, Mendoza, 5500 Argentina*

[5]*Department of Physics, Clarendon Laboratory, University of Oxford, Parks Road, Oxford OX1 3PU, United Kingdom*

(Received 5 November 2013; published 18 April 2014)

At a pressure of around 13 GPa iron undergoes a structural phase transition from the bcc to the hexagonal close-packed phase. Atomistic simulations have provided important insights into this transition. However, while experiments in polycrystals show clear evidence that the α-ϵ transition is preceded by plasticity, simulations up to now could not detect any plastic activity occurring before the phase change. Here we study shock waves in polycrystalline Fe using an interatomic potential which incorporates the α-ϵ transition faithfully. Our simulations show that the phase transformation is preceded by dislocation generation at grain boundaries, giving a three-wave profile. The α-ϵ transformation pressure is much higher than the equilibrium transformation pressure but decreases slightly with increasing loading ramp time (decreasing strain rate). The transformed phase is mostly composed of hcp grains with large defect density. Simulated x-ray diffraction displays clear evidence for this hcp phase, with powder-diffraction-type patterns as they would be seen using current experimental setups.

DOI: 10.1103/PhysRevB.89.140102 PACS number(s): 64.70.K−, 61.50.Ks, 61.72.Lk, 62.50.Ef

The study of materials under pressure is important to understand geophysical and astronomical processes but has also technological implications, for instance due to the possibility of creating new phases which might be stable at ambient conditions, with improved characteristics. In particular, there are many studies of iron under pressure, given that iron is an element of relevance in multiple areas, including its role in the Earth's core. Research using *ab initio* simulations [1], diamond anvil cells [2–4], and dynamic shock experiments [5] is achieving increasing understanding of iron phase changes at high pressure, but detailed understanding of the solid-solid phase transition occurring around 10–30 GPa is still lacking.

Shock experiments in polycrystalline Fe [6–8] in that pressure range show a three-wave structure: first the elastic compression wave, then an elastic-plastic transition, and finally the phase transition from bcc to close packed (cp). Atomistic molecular dynamic (MD) simulations have been successful in describing the bcc → cp phase transition [9–12], using the Voter embedded-atom-model (EAM) potential [13], with dislocations in the transformed cp phase [11]. However, there are outstanding issues that remain in our current understanding of shocks in Fe: Existing simulations observe purely elastic compression before the phase transformation front, even when polycrystals are considered [11], and a large fcc fraction in the simulated transformed phase, the observation of which has been elusive in experiments [14].

In this paper we go beyond previous simulations in polycrystalline Fe in several aspects: (i) we employ an EAM potential which describes both the phase transition and dislocation-based plasticity in the bcc phase, as it has been recently shown for homogeneous compression of Fe samples [15]; (ii) we implement a finite shock-loading ramp time, thus allowing for sufficient time for plasticity to build up; (iii) we employ sufficiently large grains in our nanocrystalline sample to allow for dislocation nucleation; and (iv) we calculate simulated x-ray diffraction profiles, as in a recent setup using spatial and temporal scales accessible to molecular-dynamics simulation [16]. These features allow us to obtain the experimental three-wave shock structure, alongside a large increase in transition pressure recently observed experimentally [17], and could help guide future experiments for Fe nanocrystals.

The molecular dynamics code LAMMPS [18] was used to perform the simulations. A recent review [19] studied several often-used Fe empirical potentials, comparing them to *ab-initio* calculations, including results on dislocation core structure and energy. Here, we employ a recent EAM potential, similar to the Machová and Ackland potential [20,21], but fitted specifically to provide the bcc → hcp phase transition which should occur in Fe under pressure. This potential has been described in detail recently [15] and gives a bcc → hcp transition at 13.75 GPa. We denote it as the *Ackland* potential. In addition, we performed reference simulations with the often-used Mendelev potential [22]. It provides a reasonable description of dislocation properties but does not describe properly the pressure-induced bcc → cp phase transition, since its barrier is assumed high and the transition occurs only above 60 GPa.

We have used samples containing 7–36 million atoms. Most of the simulations discussed here are for a sample with nearly 30 million atoms, with size $\sim 30 \times 30 \times 430$ nm^3. The sample was constructed with the Voronoi tesselation method [23] with a mean grain size of 7.5 nm. The cross section of the sample contains more than 10 grains, and the complete sample contains 960 grains. We relax the sample using high-temperature annealing as in Ref. [15], which is essential to equilibrate grain boundaries (GBs). The system

*urbassek@rhrk.uni-kl.de; http://www.physik.uni-kl.de/urbassek/

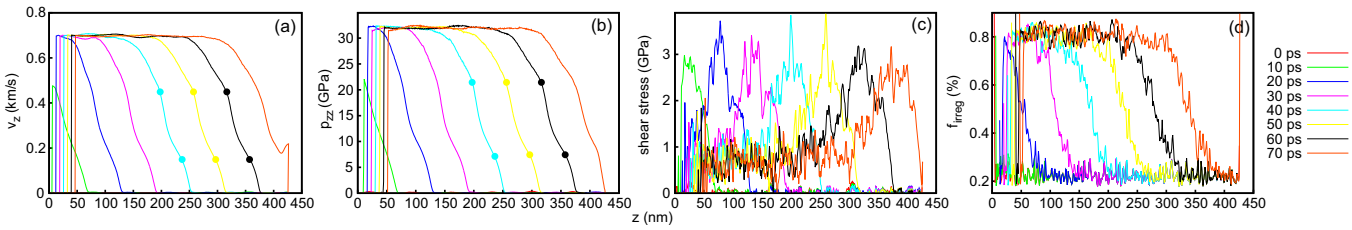

FIG. 1. (Color online) Spatial profiles of the (a) atom velocity in z direction, v_z, the (b) pressure component parallel to the shock wave propagation, p_{zz}, the (c) shear stress, and the (d) fraction of non-bcc material. The so-called knees in the profiles are marked by a dot; see text. The simulation is performed for the Ackland potential [15] and a loading rise time of 15 ps.

is initially at a temperature of 10 K. We chose this low temperature deliberately as our main aim is to look for plasticity in polycrystalline Fe: Since temperature increases under loading, a low starting temperature allows us to identify dislocations relatively easily, as thermal noise is minimal. Shocks are applied as in previous work [24], by giving a certain particle velocity to a piston on one side of the sample. This particle velocity U_p was increased linearly from zero to the desired value, 0.7 kms^{-1}, during a ramp time t_r, since nonzero rise times ease dislocation nucleation [24].

The shear stress is defined as $p_{\text{shear}} = (p_{zz} - p_{\text{trans}})/2$, where p_{ij} denote the components of the stress tensor and the transverse pressure is defined as $p_{\text{trans}} = (p_{xx} + p_{yy})/2$. A decrease in shear stress is associated with plasticity or phase transformations. Samples were visualized using common-neighbor analysis (CNA) [25,26], together with the dislocation extraction algorithm (DXA) [27,28], and the adaptive CNA algorithm contained within the open visualization tool (OVITO) and the crystal analysis tool (CAT) [29].

The space and time evolution of the quantities describing the state of the material while the shock wave passes through it are displayed in Fig. 1. The velocity profiles, $v_z(z)$, show two so-called knees—points where $v(z)$ suddenly changes slope. The knee at the front is at a particle velocity of around 0.15 kms^{-1}, while the second knee in the shocked material is at around 0.45 kms^{-1}. The knees divide the material into three sections, thus establishing the three-wave structure of the shock. The shock-wave velocity in each section is determined from Fig. 1(a) by evaluating how far the material proceeds between the different time frames shown. While the shock front moves at 6.3 kms^{-1}, the second wave moves at 5.9 kms^{-1}. Finally the wave speed in the phase-transformed material is 5.5 kms^{-1}. Those inflection points are also observed in the longitudinal stress (p_{zz}) profiles [Fig. 1(b)], the first one at $\sim$10 GPa and the second at $\sim$23 GPa. We interpret the velocity and stress profiles as having a three-wave structure: an elastic precursor wave is followed by a plastic wave, which then leads to a phase-transformation front. The Hugoniot elastic limit (HEL), which determines the transition pressure from the elastic to the plastic state, of $\sim$10 GPa agrees roughly with the threshold for dislocation emission from GBs. An HEL of $\sim$5.5 GPa was measured for a 5-μm-grain Fe polycrystal, at a strain rate of almost 10^7 s^{-1} [8]. Our simulations are carried out for 7.5-nm grains and a strain rate near 10^9 s^{-1}, both aspects leading to an increased HEL. Shear stress, Fig. 1(c), increases with compression, but in the plastic region the shear stress increase starts competing with plastic relaxation, reaching a maximum with values of 3–3.5 GPa. The plastic region is narrow due to the appearance of the phase transition. In that narrow range, there is nucleation of relatively few dislocations, as is shown later. These dislocations move only across small nanograins and do not contribute greatly to plastic relaxation. In large, micrometer-sized grains, plastic relaxation leading to nearly hydrostatic compression has been observed [14]. The fraction of non-bcc material, f_{irreg}, displayed in Fig. 1(d) reaches values of $>$80% in the shocked material. In the reference study performed with the Mendelev potential, which gives us a reference of the fraction of disordered and defective material, f_{irreg} only reaches values of around 40% [30]. The higher percentage measured for the Ackland potential is due to true phase transformation from the bcc to cp phases, which in turn includes a large amount of dislocations and stacking faults.

An analysis of the phase content shows a steady decrease of the bcc phase; the material transforms to cp phases, primarily to hcp but also some fcc [30]. Note that at these high pressures, both fcc and hcp have very similar enthalpies, so that during the nonequilibrium conditions of the shock both phases may form. In a previous study [15], we showed that after relaxation of the compressed material at a high pressure, the material will turn into hcp, while the fcc phase only appears in the form of stacking fault planes. Snapshots of the shocked sample, displaying the transformed hcp structure with fcc faults can be seen in the Supplemental Material [30].

At 70 ps, the shock wave just reached the back surface of our crystallite and is beginning to be reflected. Therefore we chose the time of 60 ps for further discussion. Figure 2 shows the relevant part of the sample. The first knee in the profiles in Fig. 1(c) is at 365 nm, marking the elastic compression wave. We observe a considerable increase of intragrain defect features at 320–280 nm, consistent with the second knee at 320 nm, marking the onset of dislocation plasticity and the start of the decrease of the shear stress. Finally the full phase transformation of grains below 280 nm leads to further reduction of the shear stress but reaches a stationary cp fraction well behind the shear stress maximum. This sequence of events gives evidence that the nucleation of the new phase is a phenomenon which is preceded by the activation of plasticity and takes time until completion after tens of picoseconds. A transition time of tens of picoseconds is well below current experimental estimates for the transition time close to 1 ns [14] for strain rates of $\sim 10^8$ s^{-1}, but a recent generation of experiments with picosecond time resolution might reduce such estimate [16]. It can be seen that the new

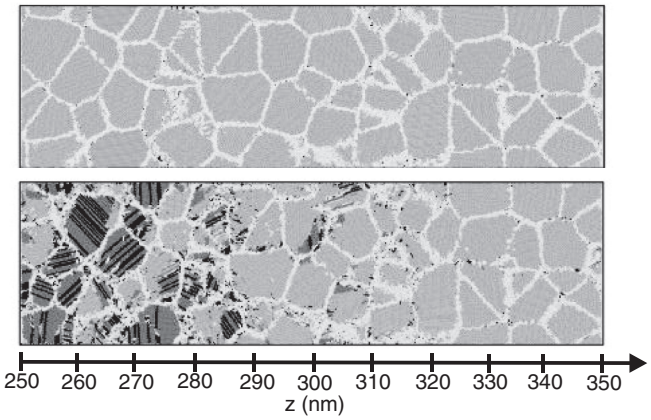

FIG. 2. Snapshots of a region of the sample extending between 250 and 350 nm from the position where the shock wave starts, before launch of the shock wave (top), and 60 ps after start of the shock wave (bottom) for the Ackland potential. Light gray: bcc; gray: hcp; black: fcc; white: other (defects, grain boundaries, etc.). Identified via adaptive CNA analysis.

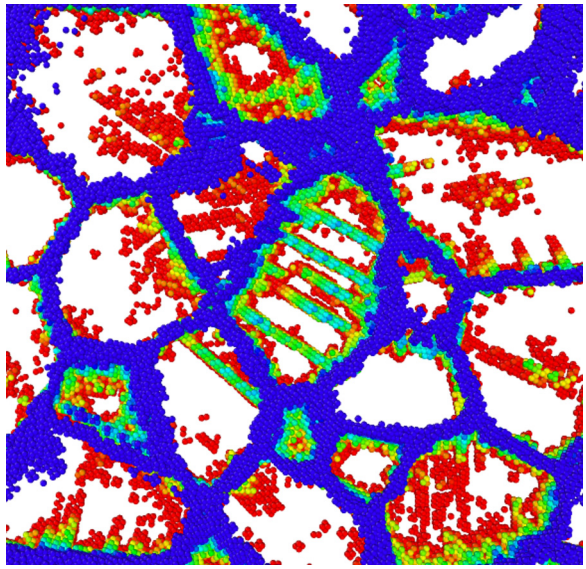

FIG. 3. (Color online) Cross-sectional view of the sample at 70 ps using the Ackland potential and the DXA tool. A slice at a depth of 381.5 nm with a thickness of 1.5 nm is shown. Only shown are atoms which belong to either GBs or dislocations or that are in otherwise strongly perturbed environment. Color code indicates depth of atoms (blue [dark gray], front; red [gray], behind). Shock wave started from behind. Note a grain containing several straight screw dislocations which have already crossed that grain. Visualization has been prepared using Ovito [31].

phase is nucleated at GBs, and therefore the grain size of the transformed grains is roughly the same as the original grain size.

An analysis of the dislocations which have formed in the material after passage of the shock wave shows that new dislocations nucleate at the GBs and then move across grains. Detailed dislocation analysis has been carried out with DXA [27,28]. A perspective view of the sample, including GBs and dislocations, can be seen in the Supplemental Material [30]. A few dislocations in this frame are shock induced and in the process of crossing grains, but several dislocation networks are just part of the structure of some GBs. Figure 3 plots a thin slice of the sample, 1.5 nm thick, in the region where there is only plasticity, just behind the elastic wave and just ahead of the phase transformation. One can see many straight dislocation segments. This is because typically a mixed dislocation loop is emitted on one side of the boundary, with the edge component advancing and leaving behind a couple of screw segments. The edge component gets absorbed at the opposite boundary, leaving the screw segments crossing the grain. This is consistent with high-resolution electron microscopy of recovered, plastically deformed bcc metals, showing mostly screw dislocations [32].

We performed a series of simulations, in which the shock ramp time t_r was varied systematically between 0.1 and 30 ps. The onset of plastic deformation does not show a dependence on ramp time, within our error bars, being 10–12 GPa. This is expected, since at these high strain rates, dislocation plasticity will depend mostly on GB structure. The onset of phase transformation, on the other hand, systematically decreases with ramp time from 26 GPa ($t_r = 0.1$ ps) to 22 GPa ($t_r = 30$ ps). Note that this transformation pressure is considerably higher than the equilibrium phase transition pressure, which is experimentally (and in the potential employed here) at 13 GPa, indicating an important role of kinetics in the phase transformation. Recent experimental results are also consistent with the phase transformation occurring above 20 GPa [17].

X-ray diffraction has proven to be a powerful tool for the ultrafast *in situ* analysis of shocked material [16]. In order to facilitate comparison of the MD results with experiments, we show in Fig. 4 simulated powder diffraction data. These were obtained by calculating the Fourier transform of the atomic coordinates, allowing interrogation of reciprocal space equivalent to that accessed in Debye-Scherrer diffraction geometries [33]. In Fig. 4(a) we show integrals around the diffraction angle ϕ, reducing the pattern to a line profile. Due to the relatively small number of grains we repeat this process for various wavelengths, summing the signals in terms of spacing d between planes. In doing so, we interrogate a larger range of reciprocal space, allowing us to capture the response of a larger number of grains. It should be noted that this procedure is strictly valid only for hydrostatic conditions, where Bragg's law provides a complete description of the relation between diffraction and strain. However, the relatively small increase in peak width and consistency of implied lattice parameters c and a of the hexagonal phase across different d imply that this assumption is valid, at least in the case of the hcp-only signal. In contrast to the values found in single-crystal shock experiments [34], our hcp phase is characterized by a lattice parameter ratio c/a of 1.6, as in the ideal hcp lattice and in recent experiments [14]. Note that the fcc phase found by CNA analysis does not display prominent features in the diffraction pattern, Fig. 4(a). In particular, the (002) peak seems to be missing in the shocked material. This is because the fcc detected by the local structural detectors (CNA) is mostly caused by stacking fault defects in the hcp phase [30]. This aspect is different from previous simulations [9–11] performed with the Voter potential, in which the fcc phase

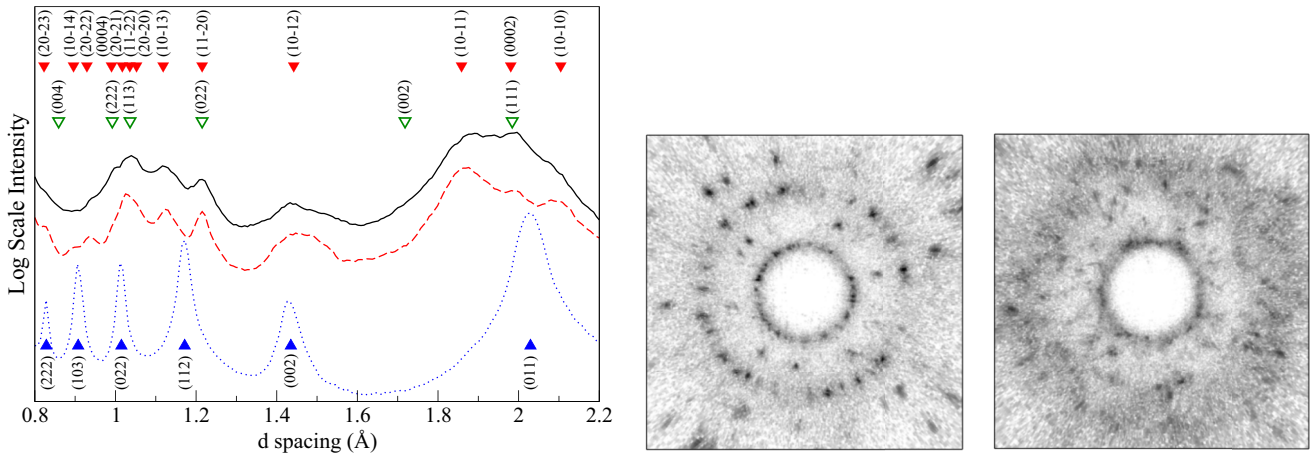

FIG. 4. (Color online) Simulated powder diffraction patterns at 70 ps. (a) Line profiles from elastically compressed (depth 400–410 nm, dotted blue [gray]) and phase changed (depth 220–230 nm, solid black) sections of the sample. The center profile (dashed red [gray]) shows the simulated diffraction profile from only those atoms in the shocked region identified as hcp by CAT. Also shown are indexing for hcp fit to the powder pattern (solid downward-facing triangles), commensurate fcc (hollow downward-facing triangles), and bcc (solid upward-facing triangles). In addition, ray tracings are displayed, simulating the diffraction patterns in an experimental geometry for (b) unshocked and (c) phase-changed sections of the sample. The diffraction pattern is simulated for a 50 × 50 mm film, placed 30 mm in transmission, using an incoming x-ray of energy 8.05 keV (Cu K_α), perpendicular to the film.

is more prominent. The fact that fcc fails to be identified is in agreement with diffraction experiments [14]. The simulated x-ray diffraction patterns feature increased ring widths during the transition accompanied by a decrease in the spot intensity from individual grains behind the phase transformation front, caused by the presence of planar faults in the transformed hcp phase, which reduce the effective grain size of the sample reducing the effective texture of the sample.

In summary, our simulations, together with a recent generation of high-pressure experiments, loading micrometer-thick films and obtaining diffraction data with time resolution of about 10 ps [16], anticipate stronger synergy between experiments and simulations covering the same length and time scales and leading to an increasing understanding of materials under extreme conditions. In particular, we show that plasticity precedes the phase transition; a polycrystalline sample with large grains and a sufficiently slow rise time of the shock are necessary for dislocations to nucleate and grow before the phase transition takes place.

This work has been supported by the Deutsche Forschungsgemeinschaft via the Sonderforschungsbereich 926. E.M.B. acknowledges support from CONICET, SeCTyP (U.N. Cuyo), and PICT-2008-1325.

[1] B. Martorell, L. Vocadlo, J. Brodholt, and I. G. Wood, Science **342**, 466 (2013).

[2] Y. Ma, E. Selvi, V. I. Levitas, and J. Hashemi, J. Phys.: Condens. Matter **18**, S1075 (2006).

[3] C. Y. Shi, L. Zhang, W. Yang, Y. Liu, J. Wang, Y. Meng, J. C. Andrews, and W. L. Mao, Nature Geosci. **6**, 971 (2013).

[4] S. Anzellini, A. Dewaele, M. Mezouar, P. Loubeyre, and G. Morard, Science **340**, 464 (2013).

[5] J. H. Nguyen and N. C. Holmes, Nature (London) **427**, 339 (2004).

[6] J. C. Boettger and D. C. Wallace, Phys. Rev. B **55**, 2840 (1997).

[7] B. J. Jensen, G. T. Gray, III, and R. S. Hixson, J. Appl. Phys. **105**, 103502 (2009).

[8] R. F. Smith, J. H. Eggert, R. E. Rudd, D. C. Swift, C. A. Bolme, and G. W. Collins, J. Appl. Phys. **110**, 123515 (2011).

[9] K. Kadau, T. C. Germann, P. S. Lomdahl, and B. L. Holian, Science **296**, 1681 (2002).

[10] K. Kadau, T. C. Germann, P. S. Lomdahl, and B. L. Holian, Phys. Rev. B **72**, 064120 (2005).

[11] K. Kadau, T. C. Germann, P. S. Lomdahl, R. C. Albers, J. S. Wark, A. Higginbotham, and B. L. Holian, Phys. Rev. Lett. **98**, 135701 (2007).

[12] B. T. Wang, J. L. Shao, G. C. Zhang, W. D. Li, and P. Zhang, J. Phys.: Condens. Matter **22**, 435404 (2010).

[13] R. J. Harrison, A. F. Voter, and S.-P. Chen, in *Atomistic Simulation of Materials: Beyond Pair Potentials*, edited by V. Vitek and D. J. Srolovitz (Plenum Press, New York, 1989), p. 219.

[14] J. A. Hawreliak, B. El-Dasher, H. Lorenzana, G. Kimminau, A. Higginbotham, B. Nagler, S. M. Vinko, W. J. Murphy, T. Whitcher, J. S. Wark, S. Rothman, and N. Park, Phys. Rev. B **83**, 144114 (2011).

[15] N. Gunkelmann, E. M. Bringa, K. Kang, G. J. Ackland, C. J. Ruestes, and H. M. Urbassek, Phys. Rev. B **86**, 144111 (2012).

[16] D. Milathianaki, S. Boutet, G. J. Williams, A. Higginbotham, D. Ratner, A. E. Gleason, M. Messerschmidt, M. M. Seibert, D. C. Swift, P. Hering, J. Robinson, W. E. White, and J. S. Wark, Science **342**, 220 (2013).

[17] Jonathan C. Crowhurst, Bryan W. Reed, Michael R. Armstrong, Harry B. Radousky, Jeffrey A. Carter, Damian C. Swift, Joseph M. Zaug, Roger W. Minich, Nick E. Teslich, and Mukul Kumar, J. Appl. Phys. **115**, 113506 (2014); R. F. Smith, J. H. Eggert, D. C. Swift, J. Wang, T. S. Duffy, D. G. Braun, R. E. Rudd, D. B. Reisman, J.-P. Davis, M. D. Knudson, and G. W. Collins, *ibid.* **114**, 223507 (2013).

[18] S. Plimpton, J. Comput. Phys. **117**, 1 (1995).

[19] L. Malerba, M. C. Marinica, N. Anento, C. Björkas, H. Nguyen, C. Domain, F. Djurabekova, P. Olsson, K. Nordlund, A. Serra, D. Terentyev, F. Willaime, and C. S. Becquart, J. Nucl. Mater. **406**, 19 (2010).

[20] A. Machov and G. J. Ackland, Modell. Simul. Mater. Sci. Eng. **6**, 521 (1998).

[21] G. J. Ackland, M. I. Mendelev, D. J. Srolovitz, S. Han, and A. V. Barashev, J. Phys.: Condens. Matter **16**, S2629 (2004).

[22] M. I. Mendelev, S. Han, D. J. Srolovitz, G. J. Ackland, D. Y. Sun, and M. Asta, Philos. Mag. **83**, 3977 (2003).

[23] A. Frøseth, H. Van Swygenhoven, and P. Derlet, Acta Mater. **53**, 4847 (2005).

[24] E. M. Bringa, K. Rosolankova, R. E. Rudd, B. A. Remington, J. S. Wark, M. Duchaineau, D. H. Kalantar, J. Hawreliak, and J. Belak, Nat. Mater. **5**, 805 (2006).

[25] D. Faken and H. Jonsson, Comput. Mater. Sci. **2**, 279 (1994).

[26] H. Tsuzuki, P. S. Branicio, and J. P. Rino, Comput. Phys. Commun. **177**, 518 (2007).

[27] A. Stukowski and K. Albe, Modell. Simul. Mater. Sci. Eng. **18**, 085001 (2010).

[28] A. Stukowski, V. V. Bulatov, and A. Arsenlis, Modell. Simul. Mater. Sci. Eng. **20**, 085007 (2012).

[29] A. Stukowski, Modell. Simul. Mater. Sci. Eng. **20**, 045021 (2012).

[30] See Supplemental Material at http://link.aps.org/supplemental/10.1103/PhysRevB.89.140102 for additional data on grain structure, dislocation activity, influence of the ramp time, and data obtained for the Mendelev potential.

[31] A. Stukowski, Modell. Simul. Mater. Sci. Eng. **18**, 015012 (2010).

[32] C.-H. Lu, B. A. Remington, B. R. Maddox, B. Kad, H.-S. Park, S. T. Prisbrey, and M. A. Meyers, Acta Mater. **60**, 6601 (2012).

[33] G. Kimminau, B. Nagler, A. Higginbotham, W. J. Murphy, N. Park, J. Hawreliak, K. Kadau, T. C. Germann, E. M. Bringa, D. H. Kalantar, H. E. Lorenzana, B. A. Remington, and J. S. Wark, J. Phys.: Condens. Matter **20**, 505203 (2008).

[34] J. Hawreliak, J. D. Colvin, J. H. Eggert, D. H. Kalantar, H. E. Lorenzana, J. S. Stölken, H. M. Davies, T. C. Germann, B. L. Holian, K. Kadau, P. S. Lomdahl, A. Higginbotham, K. Rosolankova, J. Sheppard, and J. S. Wark, Phys. Rev. B **74**, 184107 (2006).